

Supporting Information

Spill-SOS: Self-Pumping Siphon-Capillary Oil Recovery

Shenghao Wu,^{†,‡} Huachao Yang,^{†,‡} Guoping Xiong,^{§,‡} Yikuan Tian,[†] Biyao Gong,[†] Tengfei

Luo,[#] Timothy S. Fisher,[‡] Jianhua Yan,[†] Kefa Cen,[†] Zheng Bo^{†,*} and Kostya (Ken)

Ostrikov^{†,+,‡}

[†]State Key Laboratory of Clean Energy Utilization, College of Energy Engineering, Zhejiang University, Hangzhou, Zhejiang 310027, China

[§]Department of Mechanical Engineering, University of Nevada, Reno, NV 89557, USA

[#]Department of Aerospace and Mechanical Engineering, University of Notre Dame, Notre Dame, IN 46556, USA

[‡]Department of Mechanical & Aerospace Engineering and California nanoSystems Institute, University of California, Los Angeles, CA 90095, USA

⁺School of Chemistry, Physics and Mechanical Engineering, Queensland University of Technology, Brisbane, Queensland 4000, Australia

[‡]Joint CSIRO-QUT Sustainable Processes and Devices Laboratory, P. O. Box 218, Lindfield, NSW 2070, Australia

*E-mail: bozh@zju.edu.cn

Supporting Videos

Supporting Video 1 | Accelerated (720×) video of the nanostructure-enhanced oil recovery using the S-SOS device.

(Left) The oil recovery test equipped with a pristine GF sample under room environment.

(Right) The oil recovery test equipped with a VG/GF sample under room environment.

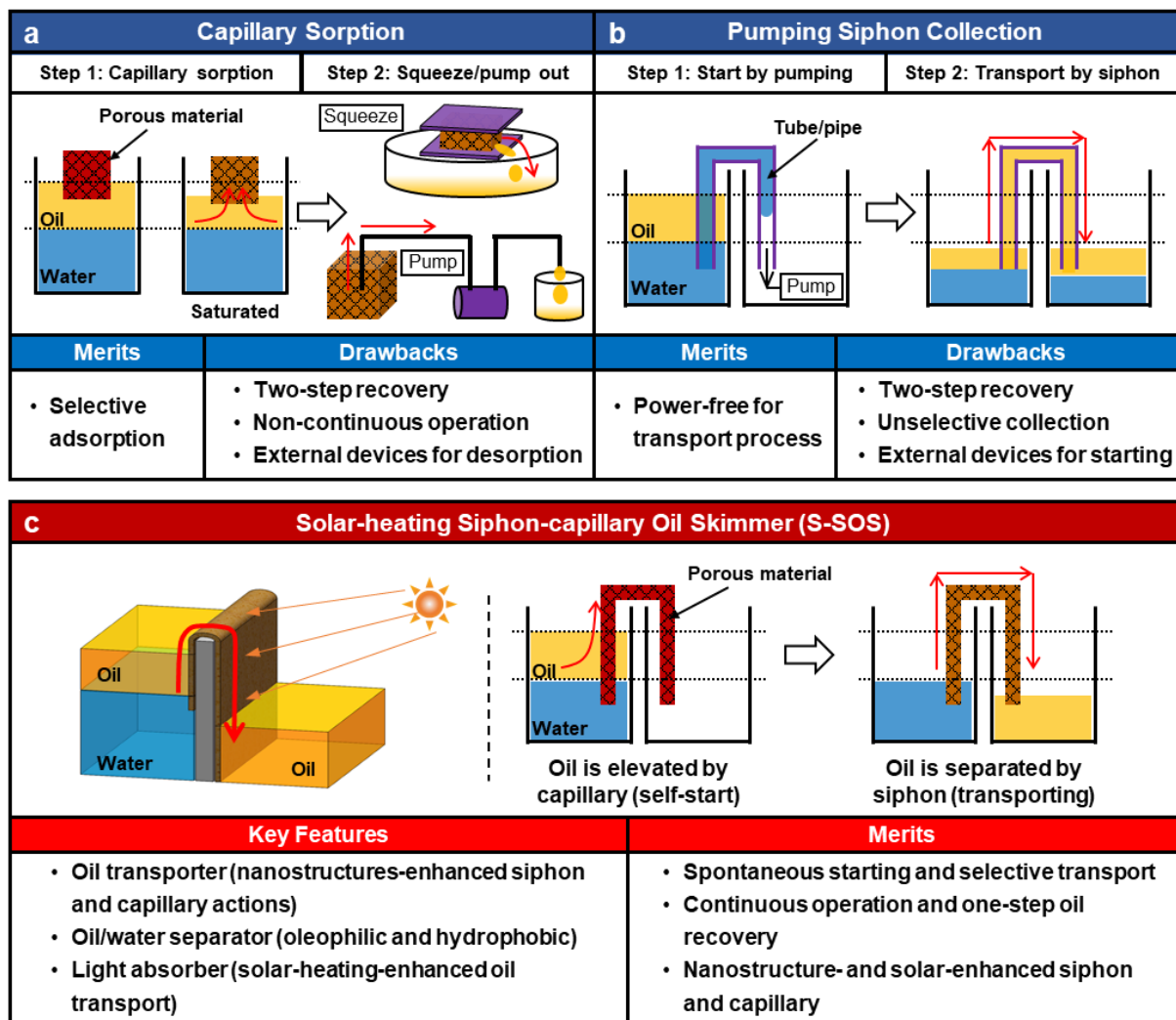
Supporting Video 2 | Accelerated (720×) video of the solar-heating-enhanced oil recovery using the S-SOS device.

(Left) The oil recovery test equipped with a VG/GF sample under room environment.

(Right) The oil recovery test equipped with a VG/GF sample under solar irradiation.

Supporting Sections

1. Comparison between the current S-SOS device and conventional oil recovery devices



Supporting Figure 1 | Comparison between the current S-SOS device and conventional oil recovery devices. (a) Conventional capillary oil-sorption device. (b) Conventional siphon transport device. (c) The current S-SOS device.

2. Concept and operation

Siphon action. Siphon is a capability of causing a liquid to flow upward above the liquid surface and then flow down due to gravity, and finally discharging it at a level lower than the liquid surface. Since this process is powered by gravitational potential energy, it presents a possibility to achieve an automatic unattended device without any external power. Previous efforts have been devoted along this direction.¹⁻² Nevertheless, the existing siphon devices still suffer from the foregoing issues of the inability to self-restart and non-selectivity.

Capillary action. Capillary is the ability of a liquid to penetrate into porous media without the assistance of, or even in opposition to, external forces like gravity. The spontaneous process is driven by solid surface energy, which has been widely applied for liquid adsorption, such as oil adsorption by porous materials.³⁻⁵ Since the capillary mainly depends on the intermolecular forces between the solid surface and surrounding liquid, by tuning the surface property, it can be achieved to selectively adsorb the oil and separate it from water.⁶⁻⁷

Taking the advantages of siphon and capillary actions together, we design an inverted U-shape porous architecture to overcome the previous issues and achieve the self-starting and selective transport for oil spill recovery. As shown in Figure 1b and Video S1, oil can spontaneously and continuously transport from one side of the wall to the other side, while water is completely prevented. The S-SOS device principally operates in two steps.

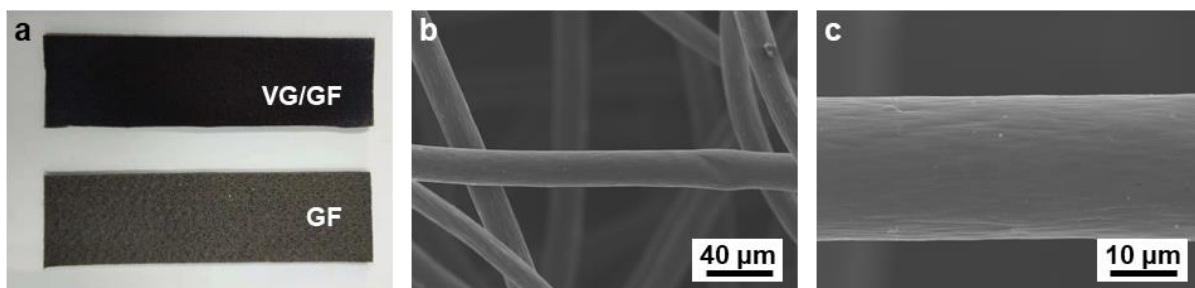
i) Self-starting by capillary action. Under capillary force, the oil afloat on the water surface spontaneously flows upward into the porous architecture, against gravity. During this process, the solid-air interface becomes the solid-oil interface, leading to a solid surface energy loss. The surface energy loss is used to drive the oil flow. When the oil reaches the plateau, gravity and capillary begin to work together to cause the oil to flow downward and completely fill the pores of the U-shape architecture. As a result, the two chambers around the

wall are connected by the oil flow, just like the continuous liquid in conventional siphon conduits.

ii) Transporting by siphon action. When the two chambers are connected by the continuous liquid (*i.e.*, the oil flow in the U-shape architecture), siphon begins to work. The oil continuously transports through the U-shape architecture and finally drops into the collecting chamber. The height difference between the upstream and the downstream results in a loss of gravitational potential energy, which is utilized to drive the oil transport. Moreover, this process will not be interrupted while exposed to the atmospheric environment. Thus, the concern of air accumulation occurring in the conventional siphon conduits is eliminated,^{1, 8} and the external device (*e.g.*, electric pump) conventionally used to help the malfunctional device return to normal operation is not needed.

Solar-heating effect. When exposed to solar irradiation, the U-shape architecture can harvest solar energy and convert it into thermal energy, leading to an increased surface temperature. When oil flows through the hot solid surface, it is heated *via* interfacial heating. As a result, the temperature of the oil flowing through the U-shape architecture is increased, leading to a decreased oil viscosity. Since the flow resistance decreases proportionally with the oil viscosity, which will be discussed in the following sections, the solar-heating and increased temperature eventually accelerate the oil recovery process.

3. Morphology of the pristine GF sample

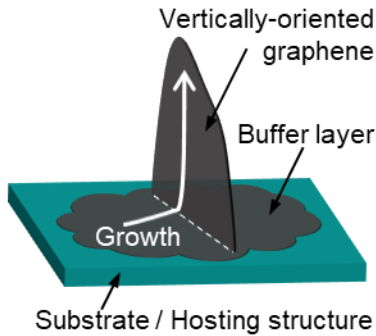


Supporting Figure 2 | Morphology of the pristine GF sample. (a) Optical images of the

VG/GF sample and the GF sample. (b) SEM image of the GF sample. (c) High-magnification SEM image of the GF sample.

4. Plasma growth mechanism

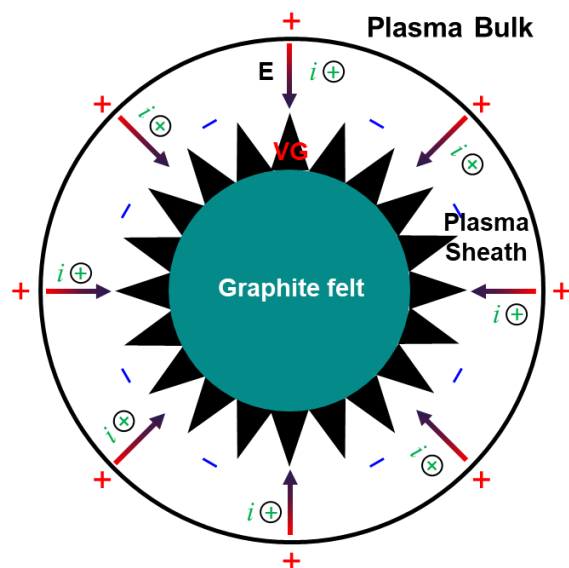
As shown in Figure S3, the vertically-oriented graphene nanosheets (*i.e.*, VGs) are perpendicularly growing from the substrate. During the growth process, a buffer layer is firstly formed on the substrate surface, serving as the nucleation sites for the subsequent VG growth. Since the growth rates in the direction perpendicular to the substrate is faster than the parallel counterpart under the plasma-made electric field, the graphene structure grows normally on the substrate, and carbon atoms are continuously incorporated into its hexagonal lattices, leading to the vertically-oriented structures.⁹⁻¹⁰



Supporting Figure 3 | Schematic of vertically-oriented structures.

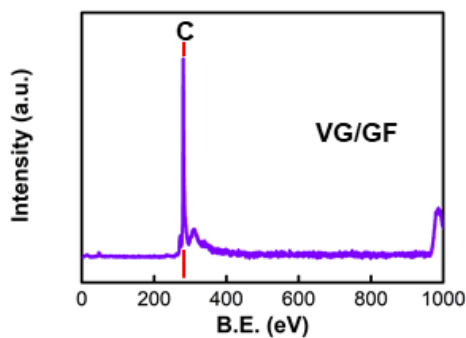
Electric field caused by gas discharges plays a crucial role on the VG growth process. As shown in Figure 2a-2e of the main manuscript, graphene structures grow normally on all the surfaces of the cylindrical carbon fibers. It is mainly attributed to the influence of the electric field in the vicinity of plasma-exposed substrate surface.¹¹ As shown in Figure S4, the GF substrate is placed in the plasma sheath, where plasma ions gain energy. The electric field sustained in the plasma sheath is used to help maintain the vertically oriented growth of the VG structures. When no substrate bias is applied, such as the PECVD system used in this

work, the potential difference across the sheath and the sheath width (equaling to a few Debye lengths) are estimated to be ~ 10 V and hundreds of micrometers,¹² respectively. Under such conditions, the plasma sheath width is much larger than the size of the VG nanostructures (with a typical height of 1-5 μm). Thus, the electric field lines converge normally onto the carbon fiber surface, leading to VG growth in the direction perpendicular to the surface of the cylindrical hosting structures. Meanwhile, the energy associated with thermal effects is estimated not to exceed 0.1 eV under the highest growth temperature of 700°C in our experiments. The low energy is insufficient to disturb and randomize the vertically oriented growth of the VG structures.¹¹



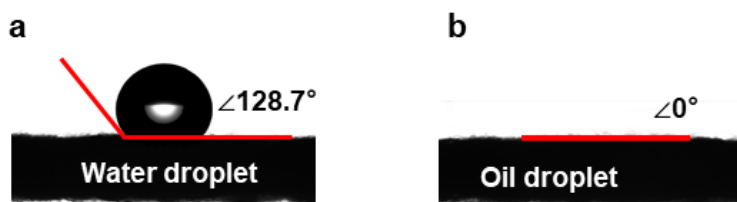
Supporting Figure 4 | Schematic of plasma sheath. The carbon fiber as a substrate of VG growth is placed in the area of the expected best plasma uniformity in a plasma discharge.

5. XPS spectrum of VG/GF



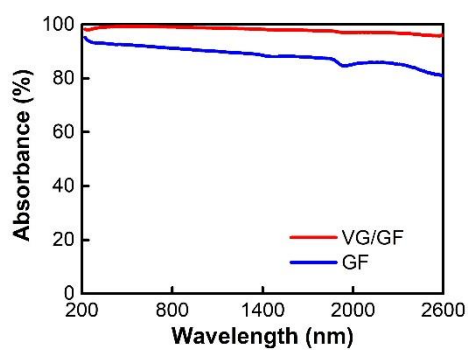
Supporting Figure 5 | XPS spectrum of VG/GF.

6. Wetting behavior of the pristine GF sample



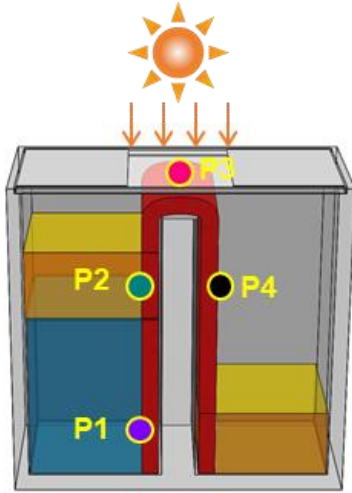
Supporting Figure 6 | Wetting behavior of the pristine GF sample. (a) Oil contact angle of the pristine GF sample. (b) Water contact angle of the pristine GF sample.

7. Comparison of photonic absorbance between VG/GF and bare GF

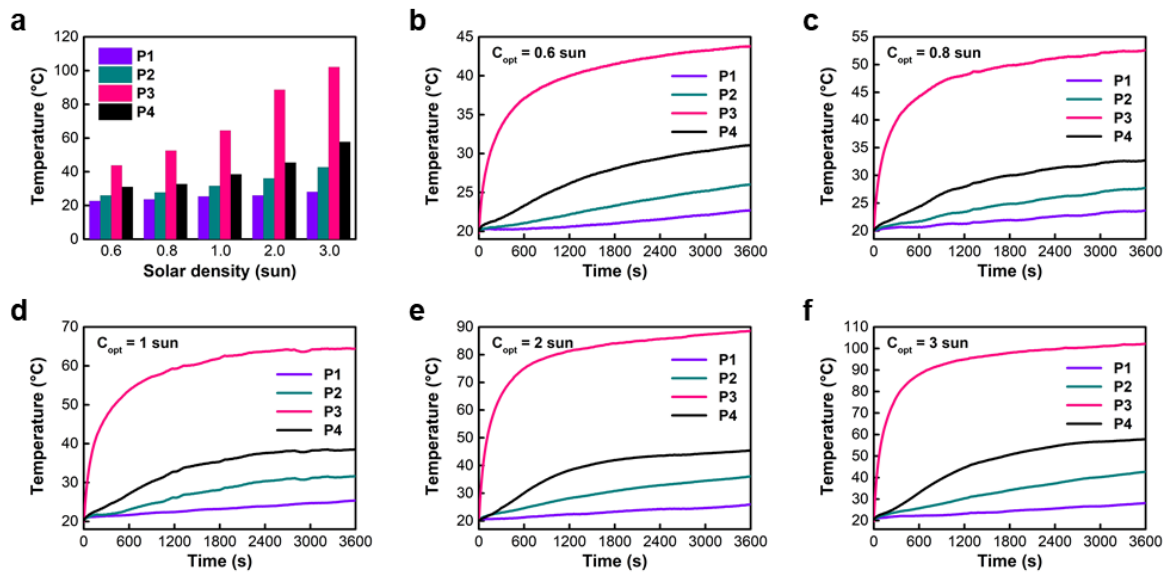


Supporting Figure 7 | Comparison of photonic absorbance between VG/GF and bare GF.

8. Temperature evolution during the oil recovery process

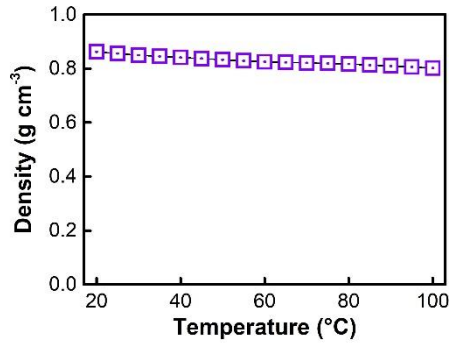


Supporting Figure 8 | Schematic of the oil temperature measurement



Supporting Figure 9 | Temperature evolutions at different points and different solar density. (a) Comparison of steady temperatures at 1 h. (b) Temperature evolutions at 0.6 sun. (c) Temperature evolutions at 0.8 sun. (d) Temperature evolutions at 1 sun. (e) Temperature evolutions at 2 sun. (f) Temperature evolutions at 3 sun.

9. Mass density of oil as a function of temperature



Supporting Figure 10 | Mass density of oil as a function of temperature

10. Analysis of force balance

As shown in Figure 4a (I), at stage i), oil permeates into the VG/GF sample and flow upward above the oil surface. The oil is pulled by capillary force (F_c) against gravity (F_g) and flow resistance (F_f), which can be expressed as:

$$m (du/dt) = F_c - F_g - F_f$$

where m denotes the oil mass, u denotes the velocity of oil flow, and t is the time. The positive sign (+) denotes the upward direction, while the negative sign (-) denotes the downward direction.

As shown in Figure 4a (II), at stage ii), oil flows downward and fills the porosity of the VG/GF sample. The two chambers are connected by the oil flow existing in the inverted U-shape architecture. The oil is pulled by capillary force and gravity against flow resistance:

$$m (dv/dt) = F_c + F_g - F_f$$

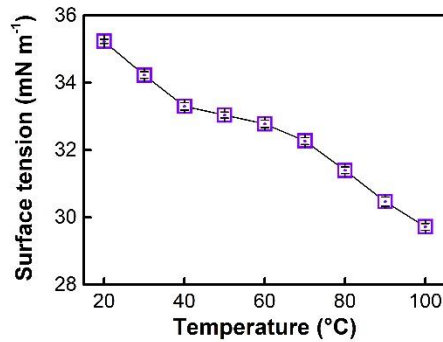
where the positive sign (+) denotes the downward direction, while the negative sign (-) denotes the upward direction.

As shown in Figure 4a (III), at stage iii), oil continuously flows through the VG/GF sample (*i.e.*, the inverted U-shape architecture), and then discharges at the right chamber (whose liquid level is lower). Based on *Bernoulli's* equation,¹ the dynamic equilibrium can be expressed as:

$$(1/2) \rho V_o^2 + \rho g H_o + P_o = (1/2) \rho V_1^2 + \rho g H_1 + P_1 + \Delta P_f$$

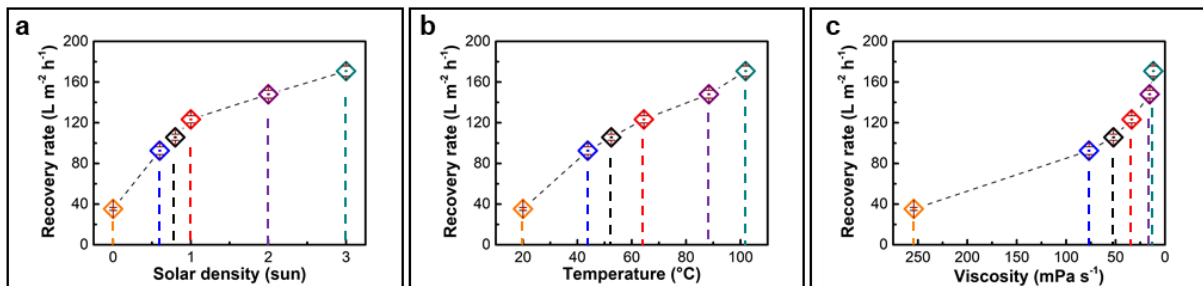
where ρ denotes the oil density, V_o and V_1 denote the oil flow velocity at upstream and downstream, respectively, H_o and H_1 denotes the height of the position at upstream and downstream, respectively, P_o and P_1 denotes the pressure at upstream and downstream, respectively, and ΔP_f denotes the total pressure drop caused by flow resistance. The upstream velocity is assumed to be zero, and the P_o and P_1 are assumed to be equal to the atmospheric pressure.

11. Surface tension of oil as a function of temperature



Supporting Figure 11 | Surface tension of oil as a function of temperature

12. Recovery rate evolution



Supporting Figure 12 | Recovery rate evolution. (a) The evolution of the oil recovery rate as a function of solar density. (b) The evolution of the oil recovery rate as a function of temperature. (c) The evolution of the oil recovery rate as a function of oil viscosity.

13. Comparison of the current S-SOS and the previous oil recovery devices

Compared with previous oil spill recovery systems,¹³⁻¹⁹ the current S-SOS device presents multiple merits, particularly in the economic cost for external devices and the energy consumption for operation, as shown in Table S1.

i) Spontaneous starting and selective transport. The S-SOS device can self-start by capillary action without the assistance of any external device. It directly reduces the economic cost for complex devices and the energy consumption to get started. Moreover, the unique surface wettability of the VG/GF allows the transport of oil and meanwhile prevents water, enabling efficient separation of oil from ocean in-situ.

ii) Continuous operation and one-step oil recovery. The S-SOS device can continuously transport oil under the siphon action without the concern of interruption. This siphon transport proceeds in a self-powered manner, where the energy from nature (*i.e.*, surface energy and gravitational potential energy) is used to drive the process. Then, the oil is directly collected from the inverted U-shape architecture without any post treatment. As a result, the power consumption for the operation process is eliminated.

iii) Nanostructure- and solar-enhanced siphon and capillary. The plasma-made graphene nanostructures can provide more siphon transport channels and enhance the capillary force to improve the oil transport behavior. Meanwhile, the VGs are capable to harvest solar energy and convert it to thermal energy to heat the oil. Consequently, the oil viscosity is reduced, eventually leading to the accelerated oil transport speed.

Supporting Table 1 | Comparison of the current S-SOS and the previous devices

Ref.	External device consuming energy			Solar irradiation	Recovery rate		Energy consumption
	Pump	Squeezer/ Centrifuge	Heater	kW m^{-2}	$\text{kg m}^{-2} \text{h}^{-1}$	$\text{L m}^{-2} \text{h}^{-1}$	kJ per kg of oil
Ref. 14	√	√	√		672.8*		54.3~74.9*
Ref.15	√					580*	<i>E</i>
Ref. 16	√	√					<i>E</i>
Ref. 17	√	√					<i>E</i>
Ref. 18	√			1.5			<i>E & S</i>
Ref. 19		√	√				<i>E</i>
Ref. 20	√	√					<i>E</i>
S-SOS, Current work	No cost for purchasing complex devices;			0	30.5	35.3	No cost for oil recovery process;
				0.6	79.8	92.5	
				0.8	91.2	105.7	
				1	106.3	123.3	
				2	127.6	148.0	
				3	147.3	170.8	

* - Estimated from the data in literatures.

E - Electricity-powered

S - Solar-powered

Meanwhile, we would like to clarify two significant difference between our work and the previous reports that also presented graphene-based materials for oil recovery.

Self-pumping recovery. In previous reports,²⁰⁻²³ the electrical pumps were often equipped to recover the oil that was adsorbed by the graphene-based sponges. These pumps required power input, such as electricity, which led to economic and energetic costs for the recovery process. In this work, we propose a self-pumping method for the oil recovery, whose process is driven by the energy from nature including solid surface energy, gravitational potential energy and solar energy. As such, the power input (*i.e.*, electricity) and the complex device (*i.e.*, electrical pump) are not required in our S-SOS device.

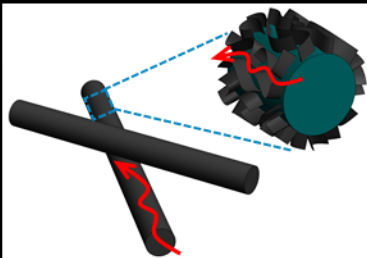
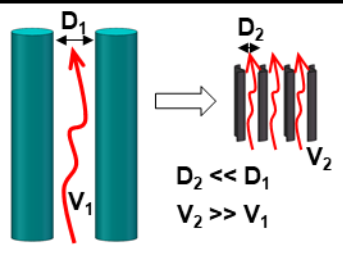
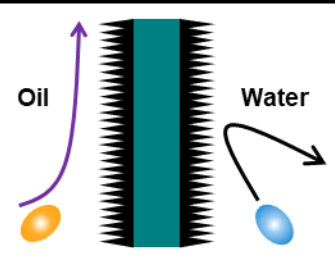
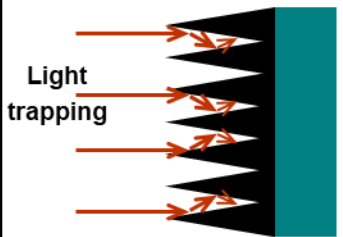
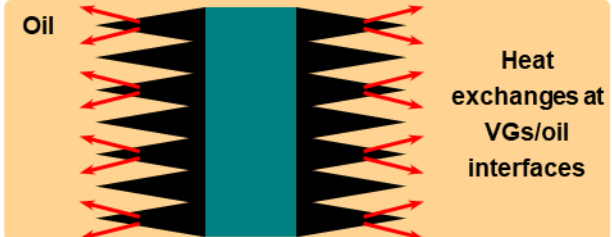
Graphene nanostructures for improved fluid transport. In previous reports, the graphene sheets were adhesive on the surface of polymer sponges by immersing the sponges in graphene oxide solution, resulting in sparsely distributed wrinkle structures on the polymer skeletons. In the current work, the graphene nanostructures are synthesized by plasma-enhanced chemical vapor deposition method, and uniformly coated on the surface of carbon fibers. Particularly, our graphene nanostructures present vertical orientation, dense nanoarrays and exposed edges, which lead to abundant channels. These graphene channels own a smaller size than the previously reported graphene structures, which leads to an enhanced capillary action and an improved fluid transport performance.

14. Crucial roles of VGs

The plasma-made VGs serve as crucial roles on the oil recovery process, as summarized in Table S2. **i) Increasing liquid channels.** The VGs with unique morphology of vertical orientation and interconnected structures can serve as flow paths for liquid. By coating the VGs on the GF to obtain the hierarchical structures, the siphon channels for oil transport is dramatically increased. **ii) Enhancing capillary action.** Since the size of the channels built by VGs ranges from tens to hundreds of nanometres, the capillary force is remarkably enhanced compared with the pristine GF sample, thus leading to a higher speed of oil transport. **iii) Tuning surface wettability.** The all-carbon structures and the high-density

edges make the VGs oleophilic and hydrophobic, sufficing the requirement of the S-SOS device. **iv) Improving light absorption.** The vertical orientation, exposed edges and dense nanoarrays make the VGs ideal candidates to trap light efficiently, maximizing the harvest of solar energy. **v) Enhancing interfacial heating.** Heat is generated in VGs by solar-thermal conversion. The exposed edges, fin-like structures as well as the good affinity between VGs and oil enable the fast heat transfer at the VGs/oil interface.

Supporting Table 2 | Summary of the advantages of VGs

Increasing liquid channels	Enhancing capillary action	Tuning surface wettability
		
Improving light absorption	Enhancing interfacial heating	
		

References

- (1) Jeong, G. S.; Oh, J.; Kim, S. B.; Dokmeci, M. R.; Bae, H.; Leede, S.-H.; Khademhosseini, A. Siphon-Driven Microfluidic Passive Pump with a Yarn Flow Resistance Controller. *Lab Chip* **2014**, *14*, 4213-4219.
- (2) Guo, Z.; Cao, Y. Spontaneous Liquid Uplift in Biliquid Capillary Siphons. *Transp. Porous Media* **2007**, *67*, 317-322.
- (3) Zhang, X.; Li, Z.; Liu, K.; Jiang, L. Bioinspired Multifunctional Foam with Self-Cleaning and Oil/Water Separation. *Adv. Funct. Mater.* **2013**, *23*, 2881-2886.
- (4) Duc Dung, N.; Tai, N.-H.; Lee, S.-B.; Kuo, W.-S. Superhydrophobic and Superoleophilic Properties of Graphene-Based Sponges Fabricated Using a Facile Dip Coating Method. *Energy Environ. Sci.* **2012**, *5*, 7908-7912.
- (5) Zhan, W.; Yu, S.; Gao, L.; Wang, F.; Fu, X.; Sui, G.; Yang, X. Bioinspired Assembly of Carbon Nanotube into Graphene Aerogel with "Cabbagelike" Hierarchical Porous Structure for Highly Efficient Organic Pollutants Cleanup. *ACS Appl. Mat. Interfaces* **2018**, *10*, 1093-1103.
- (6) Ge, J.; Zhao, H.-Y.; Zhu, H.-W.; Huang, J.; Shi, L.-A.; Yu, S.-H. Advanced Sorbents for Oil-Spill Cleanup: Recent Advances and Future Perspectives. *Adv. Mater.* **2016**, *28*, 10459-10490.
- (7) Ge, M.; Cao, C.; Huang, J.; Zhang, X.; Tang, Y.; Zhou, X.; Zhang, K.; Chen, Z.; Lai, Y. Rational Design of Materials Interface at Nanoscale Towards Intelligent Oil-Water Separation. *Nanoscale Horiz.* **2018**, *3*, 235-260.
- (8) Cai, Y.-L.; Sun, H.-Y.; Shang, Y.-Q.; Wu, Z.-J. Air Accumulation in High-Lift Siphon Hoses under the Influence of Air Dissolution and Diffusion. *J. Zhejiang Univ., Sci., A* **2015**, *16*, 760-768.
- (9) Bo, Z.; Mao, S.; Han, Z. J.; Cen, K.; Chen, J.; Ostrikov, K. Emerging Energy and Environmental Applications of Vertically-Oriented Graphenes. *Chem. Soc. Rev.* **2015**, *44*, 2108-2121.
- (10) Zhu, M.; Wang, J.; Holloway, B. C.; Outlaw, R. A.; Zhao, X.; Hou, K.; Shutthanandan, V.;

- Manos, D. M. A Mechanism for Carbon Nanosheet Formation. *Carbon* **2007**, *45*, 2229-2234.
- (11) Hatakeyama, R. Nanocarbon Materials Fabricated Using Plasmas. *Rev. Mod. Plasma Phys.* **2017**, *1*: 7.
- (12) Lin, C. C.; Leu, I. C.; Yen, J. H.; Hon, M. H. Sheath-Dependent Orientation Control of Carbon Nanofibres and Carbon Nanotubes During Plasma-Enhanced Chemical Vapour Deposition. *Nanotechnol.* **2004**, *15*, 176-179.
- (13) Ge, J.; Shi, L.-A.; Wang, Y.-C.; Zhao, H.-Y.; Yao, H.-B.; Zhu, Y.-B.; Zhang, Y.; Zhu, H.-W.; Wu, H.-A.; Yu, S.-H. Joule-Heated Graphene-Wrapped Sponge Enables Fast Clean-Up of Viscous Crude-Oil Spill. *Nat. Nanotech.* **2017**, *12*, 434-440.
- (14) He, S.; Cheng, X.; Li, Z.; Shi, X.; Yang, H.; Zhang, H. Green and Facile Synthesis of Sponge-Reinforced Silica Aerogel and Its Pumping Application for Oil Absorption. *J. Mater. Sci.* **2016**, *51*, 1292-1301.
- (15) Wang, X.; Pan, Y.; Shen, C.; Liu, C.; Liu, X. Facile Thermally Impacted Water-Induced Phase Separation Approach for the Fabrication of Skin-Free Thermoplastic Polyurethane Foam and Its Recyclable Counterpart for Oil-Water Separation. *Macromol. Rapid Commun.* **2018**, *39*, 1800635.
- (16) Khosravi, M.; Azizian, S. Synthesis of a Novel Highly Oleophilic and Highly Hydrophobic Sponge for Rapid Oil Spill Cleanup. *ACS Appl. Mat. Interfaces* **2015**, *7*, 25326-25333.
- (17) Zhang, C.; Wu, M.-B.; Wu, B.-H.; Yang, J.; Xu, Z.-K. Solar-Driven Self-Heating Sponges for Highly Efficient Crude Oil Spill Remediation. *J. Mater. Chem. A* **2018**, *6*, 8880-8885.
- (18) Liu, Y.; Shi, Q.; Hou, C.; Zhang, Q.; Li, Y.; Wang, H. Versatile Mechanically Strong and Highly Conductive Chemically Converted Graphene Aerogels. *Carbon* **2017**, *125*, 352-359.
- (19) Wang, Y.; Liu, X.; Lian, M.; Zheng, G.; Dai, K.; Guo, Z.; Liu, C.; Shen, C. Continuous Fabrication of Polymer Microfiber Bundles with Interconnected Microchannels for Oil/Water Separation. *Appl. Mater. Today* **2017**, *9*, 77-81.

- (20) Jiang, Z.-R.; Ge, J.; Zhou, Y.-X.; Wang, Z. U.; Chen, D.; Yu, S.-H.; Jiang, H.-L. Coating Sponge with a Hydrophobic Porous Coordination Polymer Containing a Low-Energy CF₃-Decorated Surface for Continuous Pumping Recovery of an Oil Spill from Water. *NPG Asia Mater.* **2016**, 8, e253.
- (21) Wang, Y.; Zhou, L.; Luo, X.; Zhang, Y.; Sun, J.; Ning, X.; Yuan, Y. Solar-Heated Graphene Sponge for High-Efficiency Clean-Up of Viscous Crude Oil Spill. *J. Clean. Prod.* **2019**, 230, 995-1002.
- (22) Zhang, L.; Li, H.; Lai, X.; Su, X.; Liang, T.; Zeng, X. Thiolated Graphene-Based Superhydrophobic Sponges for Oil-Water Separation. *Chem. Eng. J.* **2017**, 316, 736-743.
- (23) Luo, Y.; Jiang, S.; Xiao, Q.; Chen, C.; Li, B. Highly Reusable and Superhydrophobic Spongy Graphene Aerogels for Efficient Oil/Water Separation. *Sci. Rep.* **2017**, 7, 7162.